ACCEPTED VERSION

Ng, C.T.; Veidt, M.
A Lamb-wave-based technique for damage detection in composite laminates, *Smart Materials & Structures*, 2009; 18(7):1-12.

© 2009 IOP Publishing Ltd.

DOI: 10.1088/0964-1726/18/7/074006

PERMISSIONS

http://iopscience.iop.org/0964-1726/page/Open%20access%20information

Open access information

- Authors who do not select the gold open access option can post the accepted version of their manuscript to an institutional or subject repository after a 12 month embargo (with reuse restrictions). The accepted version of a paper refers to an author's original version of an article after any changes made during peer review but before any editing, typesetting, etc by the publisher.

8th October, 2014

http://hdl.handle.net/2440/64625

A Lamb wave based technique for damage detection in composite laminates

C T Ng[1,2] and M Veidt[1]

[1] School of Engineering, The University of Queensland, Brisbane, Qld, 4072

[2] Cooperative Research Centre for Advanced Composite Structures Ltd, Fishermans Bend, Vic, 3201

Email: m.veidt@uq.edu.au

Abstract. This paper presents the application of Lamb waves to inspect damage in composite laminates. The proposed methodology employs a network of transducers that are used to sequentially scan the structure before and after the presence of damage by transmitting and receiving Lamb wave pulses. A damage localization image is reconstructed by analyzing the cross correlation of the scatter signal envelope with the excitation pulse envelope for each transducer pair. A potential damage area is then reconstructed by superimposing the image observed from each actuator and sensor signal path. Both numerical and experimental case studies are used to verify the proposed methodology for composite laminates. Three-dimensional finite element models with a transducer network consisting four transducer elements are used in the numerical case studies. The experimental case studies employ a transducer network using four piezoelectric transducers as transmitter elements and a laser vibrometer to measure the response signals at four locations close to the transducers. The results show that the method enables the reliable detection of structural damage with locating inaccuracies in the order of a few millimeters inside as well as outside of an inspection area of 100 x 100 mm^2.

1. Introduction

The importance of structural health monitoring (SHM) to enhance the reliability and reduce the life-cycle costs of current and future infrastructure is widely recognized. Low-frequency damage detection methods that utilize modal characteristics (Cawley and Adams 1979) or time domain dynamic responses (Lam *et al* 2007, Lam and Ng 2008) have been a commonly used approach in SHM. Although this approach enables global monitoring, the low-frequency characteristics are usually insensitive to small damage. Recently, Lamb wave based SHM methodologies have been widely reported to be sensitive to small damage, convenient and efficient in detecting fatigue cracks in metallic structures, disbonds and delaminations in composite structures and for the assessment of structural repairs, e.g. (Boller 2000, Diamanti *et al* 2004, Su *et al* 2006, Raghavan and Cesnik 2007, Diamanti *et al* 2007, Worden *et al* 2007, Ihn and Chang 2008).

Apart from the essential requirement that SHM systems must be reliable, two important desired features are graphical representation and quantitative evaluation of damage. In the literature, different methods have been developed to provide a graphical representation of damage. Lin and Yuan (2001) applied the migration technique, which has been widely employed in geophysical exploration, to detect and produce an image for damaged plates. A numerical study using a linear transducer array on an isotropic plate was used to verify the method. Wang *et al* (2004) presented an imaging method based on the time-reversal concept for damage detection and the method was experimentally verified using an aluminum plate. Zhao *et al* (2007) developed a reconstruction algorithm for probabilistic inspection of defects (RAPID) for damage detection in an aircraft wing using ultrasonic guided waves. A defect distribution probability map is constructed to locate the damage and to monitor its growth. The method was verified using an aircraft wing made from aluminum alloys and coated with paint. Michaels and Michaels (2007) applied time shift averaging algorithms to differential Lamb wave signals filtered at multiple frequencies. A set of images corresponding to each

centre frequency are then generated and combined to form an image for locating the damage. An experimental verification was carried out using an aluminum plate. Su *et al* (2008) proposed an imaging method for damage detection using Lamb waves. Probability densities of damage occurrence are calculated based on time of flight analysis of scatter waves and superimposed to form an image of the damaged composite laminate.

Beam forming is a sensor array signal processing technique which has been applied in different fields, e.g. sonar systems (Curtis and Ward 1980), wireless communications (Litva and Lo 1996) and nondestructive testing (Ghorayeb *et al* 1994). Recently, the beam forming technique has been applied to damage detection using Lamb waves. Giurgiutiu and Bao (2004) used embedded-ultrasonic structural radar and phased-array beam forming techniques for damage detection. Experimental studies were carried out on metallic structures to illustrate and verify the method. Sundararaman *et al* (2005) employed beamformers consisting of sparse phased array transducers to characterize damage in homogeneous and heterogeneous structures. Olson *et al* (2007) applied beam forming and an array of piezoelectric transducers to detect damage and an experimental study using an aluminum plate was used to verify the method.

This paper addresses a number of extensions to the current status of Lamb wave beam forming. It systematically investigates the application of the method to detect and locate damage in composite laminates by accounting for the angular dependence of the group velocity. It introduces a graphical representation that not only pinpoints the location of damage but reconstructs a possible damage area which provides quantitative information with the potential to assess the need for any required remedial work. It systematically evaluates and validates the robustness of the method for damage located at different positions relative to the transducer network area in numerical and experimental case studies and quantifies damage localization errors.

The proposed methodology employs a network of transducers that are used to

sequentially scan the structure before and after the presence of damage. A damage localization image is then reconstructed by analyzing the cross correlation between the envelope of the scatter wave and the excitation pulse applying the fundamental framework of digital beam forming. The organization of this paper is as follows: The methodology section introduces the fundamentals of the beam forming framework, describes the Hilbert transform signal processing technique, which is employed to calculate the envelope of the scatter pulse and briefly discusses some aspects of the explicit finite element method that is used in the numerical case studies. The potential of the methodology to detect and locate damage in composite laminates and its robustness and accuracy are illustrated by the results of numerical and experimental cases studies presented in sections 3 and 4, followed by conclusions in section 5.

2. Methodology

2.1. Lamb wave based damage detection technique for anisotropic material

The Lamb wave based damage detection methodology for anisotropic materials is based on the fundamental idea of beam forming which is illustrated in the Figure 1. Figure 1a shows two transducers a and b which are members of a distributed transducer network with N transducers. Each of the transducers can act as both actuator and sensor for excitation and measurement, respectively. A sequential scan for detecting damage in large structures can thus be performed by exciting one of the transducers, e.g. transducer a to generate a Lamb wave while the rest of the transducers, e.g. transducer b, are used for measuring the impinging waves. This results in a total of $N(N-1)$ actuator/sensor signal paths. When the Lamb wave interacts with the damage, wave scattering occurs. The scatter signal is obtained using baseline subtraction as

$$\mathbf{u}_{ab}^{(S)} = \mathbf{u}_{ab}^{(D)} - \mathbf{u}_{ab}^{(I)} \tag{1}$$

where $\mathbf{u}_{ab}^{(S)}$ and $\mathbf{u}_{ab}^{(I)}$ are the vectors of the scatter and incident signals, respectively and $\mathbf{u}_{ab}^{(D)}$ is the signal vector for the damaged structure. The proposed Lamb wave based damage detection methodology utilizes the scatter wave signals $\mathbf{u}_{ab}^{(S)}$ to reconstruct a damage localization image.

As shown in Figure 1b, the inspection area is discretized into a set of imaging pixel (x, y). Based on the known positions of the actuator, sensor and imaging pixel location and the velocity of the Lamb wave, a time shift describing the location of the scattering source is determined using the cross-correlation between the envelope of the scatter wave and the excitation pulse for each actuator and sensor signal path as

$$C_{ab}(t) = \int_0^T \hat{u}_{ab}^{(S)}(\tau)\hat{F}(\tau + t)d\tau \tag{2}$$

where $\hat{u}_{ab}^{(S)}$ is the envelope of the scatter signal in which transducer a and b act as actuator and sensor, respectively. T is the duration of the scatter signal and $\hat{F}$ is the envelope of the excitation pulse. Both envelopes are obtained using Hilbert transform signal processing as described in the next sub-section. The arrival time of the scattered wave corresponds to the wave travel time from the actuator to the damage and then from the damage to sensor.

$$T_{ab}(x, y) = \frac{d_a(x, y)}{c_g(\theta_a)} + \frac{d_b(x, y)}{c_g(\theta_b)} \tag{3}$$

where d_a and d_b are the distance from the transducer a (actuator) to the damage and from the damage to the transducer b (sensor), respectively. $c_g(\theta)$ is the group velocity of the Lamb wave, which in general depends on the propagation direction θ. θ_a and θ_b describe the wave propagation direction from transducer a to the damage and from the damage to transducer b, respectively. For each actuator and sensor signal path, the value of the cross correlation at possible damage locations is much higher than at other imaging pixels.

For isotropic materials, imaging pixels with identical relative intensity form ellipses for each actuator and sensor transducer pair (Veidt *et al* 2008). This will not be the case for anisotropic materials, since the velocity of the interrogating wave depends on the propagation direction. The reconstructed damage localization image is created by superimposing the power flux of all actuator and sensor signal path images as

$$I(x,y)=\sum_{a=1}^{N}\sum_{b=1,b\neq a}^{N}A_{ab}\left[C_{ab}\left(T_{ab}(x,y)\right)\right]^2 \tag{4}$$

where A_{ab} are weighting factors to account for varying sensitivities of individual transducers and which are equal to unity for uniform aperture weighting. Based on the fundamental idea of the beam forming technique, the signal-to-noise ratio of the reconstructed damage localization image is greatly improved due to the summation of all the actuator and sensor signal path images.

2.2. Hilbert transform

The Hilbert transform of an arbitrary time series $w(t)$ is defined as, e.g. (Staszewski *et al* 2004)

$$\mathcal{H}(t)=\frac{1}{\pi}\int_{-\infty}^{\infty}\frac{w(\tau)}{t-\tau}d\tau \tag{5}$$

The transformed series $\mathcal{H}(t)$ is a 90^{o} phase shift of the arbitrary time series $w(t)$. An analytic signal is constructed by using the arbitrary time series $w(t)$ as real and the Hilbert transformed series $\mathcal{H}(t)$ as imaginary part.

$$w_A(t)=w(t)+j\mathcal{H}(t)=\hat{w}(t)e^{j\phi(t)} \tag{6}$$

where j is the imaginary unit. $\hat{w}(t)$ and $\phi(t)$ are envelope and instantaneous phase and are defined as

$$\hat{w}(t)=\sqrt{w^2(t)+\mathcal{H}^2(t)},\qquad \phi(t)=\arctan\left[\frac{\mathcal{H}(t)}{w(t)}\right] \tag{7}$$

The envelopes of the scatter wave and the excitation pulse are obtained using Hilbert transform signal processing which are then employed to reconstruct the damage using the proposed Lamb wave based damage detection methodology.

3. Numerical case studies

The aim of the numerical studies is to systematically investigate the robustness of the proposed Lamb wave based damage detection methodology for anisotropic composite laminates. The finite element method (FEM) is employed to simulate Lamb wave propagation and scattering. The Lamb wave propagation is a local dynamic effect that depends on the wave propagation distance from the excitation point. Without loss of generality, one part of the transducer network that is formed by four transducer elements is simulated with all edges are assumed to be free (as shown in Figure 2). The test system consists of an 8-ply $[0_8]$ carbon fiber-reinforced composite laminate with dimension $250 \times 250 \times 1.6\ mm^3$. The material properties of the lamina are summarized in table 1. According to the coordinate system shown in Figure 2, four transducers $T_1 - T_4$ are surface mounted on the composite laminate at ($x_1 = 165\ mm$, $y_1 = 150\ mm$), ($x_2 = 85\ mm$, $y_2 = 150\ mm$), ($x_3 = 85\ mm$, $y_3 = 125\ mm$) and ($x_4 = 165\ mm$, $y_4 = 125\ mm$), respectively, to form a rectangular monitoring area. As the installed transducers represent the geometric change within the laminate, they act as wave scatterers. Hence they are included in the finite element model but only as elastic inhomogeneities and not as electro-mechanical elements. The geometric and material properties of the transducer are summarized in table 2. The first antisymmetric Lamb wave is excited by applying a uniform pressure at the contact surface between the transducer and the laminate. The excitation consists of a 200 kHz narrow-band four cycle sinusoidal tone burst modulated by a Hanning window. Through hole damage is considered in the numerical case studies.

Both composite laminate and transducers are modeled using three-dimensional

eight-node brick elements C3D8R (ABAQUS Theory Manual 2007) in which each node has three degrees-of-freedom (DoF). The element size is limited to guarantee ten nodes exist per wavelength (Alleyne and Cawley 1991) and the composite laminate is divided into two layers through the thickness. This results in approximately 370,000 elements and 555,000 DoFs in total. The dynamic analysis is solved by using ABAQUS/Explicit. ABAQUS/Explicit employs the explicit central different integration scheme to calculate the response of the wave propagation. As the central different integration scheme is only conditionally stable, the maximum increment time step $\Delta t_{\max}$ in the central different integration scheme has to be small enough to ensure stability. It is controlled by

$$\Delta t_{\max} \leq \frac{L_{\min}}{c_{\max}} \tag{8}$$

where $c_{\max}$ is the maximum longitudinal wave velocity in the composite laminate (i.e. in 0^{o} direction) and $L_{\min}$ is smallest element length in the finite element model. The smallest element length in the numerical investigations is approximately $0.29\,mm$. The maximum longitudinal wave velocity $c_{\max}$ is calculated using the software DISPERSE (Pavlakovic and Lowe 2003) and is $9960\,m/s$. Hence, the maximum allowable time step increment $\Delta t_{\max}$ according to equation (8) is 2.91×10^{-8} seconds. All finite element simulations presented in this study are carried out using a sample rate of 100MHz to ensure the stability of the central different integration scheme. Bulk viscosity is considered in the ABAQUS/Explicit analysis to introduce a damping effect associated with the volumetric straining and to improve the modeling of the wave propagation.

For demonstration purpose, a sequence of out-of-plane displacement fields are shown in Figure 3, which shows an area of the laminate around transducer T_2, to illustrate the Lamb wave propagation and scattering in the composite laminate. For clarity reasons, the damage is located relatively close to transducer T_2 at ($x_d = 115\,mm$, $y_d = 150\,mm$) in order to avoid scatter waves from boundaries and other transducers. Figure 3a shows how the Lamb wave

propagates in all directions according to the directionally dependent group velocity, which is shown in Figure 4. The group velocity is obtained by evaluating the time-of-flight of the simulated wave package propagating in different directions, i.e. following the same procedure that is used experimentally. The figure shows that the group velocity of the first antisymmetric Lamb mode at 200 kHz varies between 1708.10 m/s in the fiber direction and 1354.40 m/s in the direction perpendicular to the fibers. Figures 3b and c show the scattering of the wave at the through hole and Figure 3d shows the interaction of the scatter wave with the excitation transducer. Figure 5 shows time histories measured at the centre of the excitation transducer. The baseline signal without any damage and the total signal with the through hole damage can be seen in Figure 5a. The scatter signal in Figure 5b is determined using baseline subtraction according to equation (1). Since all signal amplitudes are normalized with respect to the maximum value of the baseline signal the figure shows that the maximum scatter signal amplitude is approximately 10% or -20dB of the baseline amplitude.

3.1. Damage detection results

Five cases N1 – N5 are considered in the numerical case studies. The damage characteristics are summarized in table 3. Cases N1 – N3 consider damage located at (x_d = 135.00 mm , y_d = 135.00 mm), i.e. slightly off-centre within the transducer network area, but with different diameters of the through holes, namely 2.00 mm in case N1, 1.00 mm in case N2 and 0.50 mm in case N3. Case N4 considers a 1.00 mm diameter through hole located at (x_d = 155.00 mm , y_d = 145.00 mm). The purpose of case N4 is to investigate the robustness of the proposed methodology in a situation where the damage is relatively close to one of the transducers. Case N5 also considers a 1.0 mm diameter through hole but this time located at (x_d = 175 mm , y_d = 130 mm), i.e. slightly outside of the transducer network area.

The reconstructed damage localization image of case N1 is shown in Figure 6. Figure 6a

shows the reconstructed damage localization image. The white squares indicate the transducer locations and the purple circle is the true damage location. It shows that the reconstructed damage localization image accurately locates the damage. This damage reconstruction is obtained by superposing the images of different actuator/sensor signal paths as explained in section 2.1. Figures 6c and d show as examples the actuator/sensor signal path T_1-T_2 and T_1-T_4, respectively, and illustrate that they are no longer perfect ellipses as in the case of an isotropic material. Figure 6b shows a binary image created from Figure 6a by only accounting image pixels whose intensity is larger than an arbitrarily threshold value, which in this study was chosen as 95% of the maximum intensity of the reconstructed damage localization image. The aim of the binary image is: i) to provide a robust damage localization image by filtering out minor intensity peaks which may occur; ii) to indicate the width of the maximum intensity peak which can be used as a measure of the uncertainty of damage detection; and iii) to determine the predicted damage location by calculating its centroid as the ratio of the first- and zeroth-order spatial moments of the binary image (Pratt 1991). The predicted damage location is listed in the fourth column in table 3. Figure 7 shows the sectional view of the reconstructed image along the x and y directions through the actual damage position. Both figures show the reconstructed localization image accurately located the damage. The predicted damage location for case N1 is (x_c = 135.32 mm, y_c = 135.95 mm) which is very close to the true location. The damage locating error E shown in the fifth column of table 3 is defined as $E=\sqrt{(x_c-x_d)^2+(y_c-y_d)^2}$ which in case N1 is E = 1.00 mm.

The reconstructed damage localization image of cases N2 and N3 are shown in Figures 8a and b. The through holes are accurately located in both cases with locating errors of 1.09 mm for case N2 and 1.45 mm for case N3. The difference in prediction accuracy between cases N1, N2 and N3 are the result of different scattering patterns which are a

function of the characteristic length scale ka with k the wave number of the incident wave and a the diameter of the damage (Rohde *et al.* 2007, Cegla *et al.* 2008).

Case N4 aims to study the performance of Lamb wave based damage detection methodology under a situation where the damage is located relatively close to one of the transducers in order to verify the robustness of the proposed methodology. Figure 9 shows the reconstructed damage localization image and corresponding binary image. Although Figure 9a shows an elongated area of high intensity amplitude, the 95% binary image depicted in Figure 9b still has a circular shape and is located relatively close to the true damage. Table 3 shows that the damage locating error E is below 5 mm .

The last case of the numerical case study is case N5 and it is used to study the performance when the damage is located outside of the transducer network. The reconstructed damage localization image and corresponding binary image are shown in Figure 10. This case again highlights the robustness of detecting and locating damage in composite laminates using the proposed Lamb wave based damage detection methodology with a locating error $E = 2.34\,mm$.

A sensitivity study has been carried out by Veidt *et al*. (2008) using a simplified numerical simulation model, which is accounting for the angular dependence of the group velocity in a composite laminate but is not considering the detailed scatter field distribution. It shows that the damage location error is of the order of 2 mm and 8 mm when the damage is located within the transducer network and very close to one of the transducers, respectively. The current study extends this work by considering the correct scatter field distributions and damage located at representative locations, namely in cases N2, N4 and N5 in which the damage is located within the transducer network, relatively close to one of the transducers and outside the transducer network. The results show that the distribution of the damage location error is consistent with the results in Veidt *et al*. (2008) with small damage location error ($E = 1.09\,mm$ in case N2) for damage located within the transducer network. The

damage location error becomes larger when the damage is closer to one of the transducers (E = 4.85 mm in case N4) or outside of the transducer network (E = 2.43 mm in case N5).

4. Experimental Studies

The aim of the experimental studies is to validate the predictions from the simulation studies and to identify practical issues, which have to be solved before the Lamb wave based damage detection methodology can be used to design multifunctional, smart structures for in-situ SHM. The proposed methodology is verified using a 16-ply $[(0/90)_4]_s$ composite laminate with dimensions $615 \times 615 \times 3.3\ mm^3$. The laminate is fabricated from Cycom ®970 unidirectional carbon/epoxy prepreg tape. Four piezoceramic disk actuators $T_1 - T_4$, (Ferroperm Pz27, 5 mm diameter, 2 mm thickness, 3 mm thick brass backing mass), are adhesively bonded to the composite laminate at positions (x_1 = 90 mm, y_1 = 80 mm), (x_2 = 10 mm, y_2 = 90 mm), (x_3 = 10 mm, y_3 = 10 mm) and (x_4 = 80 mm, y_4 = 20 mm) to form a representative cell of a distributed sensor network, Figure 11a. The excitation is a 200 kHz, eight cycle sinusoidal tone burst modulated by a Hanning window. The Lamb wave signal excited by the piezoeramic disk actuator is measured using a heterodyne laser Doppler vibrometer Polytec OFV303, Figure 11b, at measurement locations 10 mm away from the centre of the actuators in both x and y direction. The four measurement locations $M_1 - M_4$ are at (x_1 = 80 mm, y_1 = 70 mm), (x_2 = 20 mm, y_2 = 80 mm), (x_3 = 20 mm, y_3 = 20 mm) and (x_4 = 70 mm, y_4 = 30 mm), respectively. It has been shown by Mallet *et al.* (2004) that the response signal collected by laser vibrometer and piezoelectric transducer are practically identical. Hence the damage localization results for the experimental case studies presented in the following section using the laser vibrometer as non-contact, optical sensor are considered to be representative to assess the accuracy and robustness of the methodology. Transducer geometry and the frequency content of the excitation signal are determined in

preliminary experiments that investigate the transduction efficiency of the transducers (Veidt *et al*. 2001; Santoni *et al*. 2007) with the aim to optimize signal-to-noise ratio, limit dispersive effects of the interrogating pulse and avoid the propagation of multiple modes. The sampling frequency is set at 5 MHz. The measured baseline and total signal, the calculated scatter signal and the corresponding signal envelope are shown in Figure 12 for a $10\,mm$ diameter, $4\,mm$ thick bonded mass as artificial damage for excitation at T_3 and measurement location M_2. All signals are normalized by the maximum amplitude of the baseline signal. The scatter wave is calculated using baseline subtraction according to equation (1). The maximum amplitude is approximately 10% of the baseline amplitude which is similar to the scatter signals considered in the numerical case studies.

Figure 13 shows the angular dependence of group velocity which is obtained by measuring the time-of-flight of the Lamb wave propagating in different directions. The measured angular dependence of the group velocity is employed in the beam forming procedure to detect and locate the damage. The reason why the group velocity does not explicitly show a pronounced directional dependence is that at 200 kHz the propagation behavior of the first antisymmetric Lamb wave in the cross-ply laminate is mainly dependent on the out-of-plane shear modulus of the material which is almost the same for all propagation directions.

4.1. Damage detection results

Four cases E1 – E4 are considered in the experimental case studies and are summarized in Table 4. Previous studies (Wang and Chang 2005; Cegla *et al*. 2008) have shown that scatter field distributions are not very sensitive to the amount of stiffness change but that the major parameter influencing the scatter field is the ratio between the wavelength of the interrogating wave and the damage size. The damage is thus simulated by adhesively bonding a brass mass on one side of the composite laminate to cause a change of flexural stiffness, extensional

stiffness and inertia at the location of the bonded mass. Wang *et al*. (2004) have shown that the scatter field caused by a bonded mass is representative of the one caused by a delamination in the case of an interrogating wave consisting of the first antisymmetric Lamb wave mode. Cases E1 and E2 both consider the damage located at ($x_d = 55.00\,mm$, $y_d = 60.00\,mm$). Case E1 uses a bonded mass of $10\,mm$ diameter and $5\,mm$ thickness whereas the mass in case E2 has a diameter of $5\,mm$ and a thickness of $3\,mm$. Cases E3 and E4 use a $5\,mm$ diameter bonded mass attached at different locations. In case E3 the damage is located close to transducer T2 at ($x_d = 10.00\,mm$, $y_d = 80.00\,mm$). This case is used to investigate the ability of the proposed methodology to detect damage that is located close to one of the transducers of the network which results in more complex scattering signals due to the scatter waves generated at the transducer which interfere with the scatter from the damage. Case E4 considers the situation when the damage is located outside of the transducer network ($x_d = 55.00\,mm$, $y_d = 90.00\,mm$) and is used to further investigate the robustness of the proposed methodology.

Figure 14 shows the reconstructed damage localization image and corresponding binary image for case E1. The white squares and triangles show the locations of the transducers and laser measurement points, respectively, while the purple circle indicates the location and size of the bonded mass. It can be seen from the reconstructed localization image that the estimated damage is almost exactly the same as the true damage, especially in the binary image. The locating error E is $0.17\,mm$, Table 4. The corresponding image for case E2 with the 5 mm diameter bonded mass is shown in Figure 15. The images show that accurate location is also possible for the small mass although the locating error $E = 4.44\,mm$ is considerably larger than for case E1.

Figures 16a and b show the reconstructed damage localization image and corresponding binary image of case E3. Both images accurately indicate the bonded mass location, especially the binary image. The damage locating error E is $2.09\,mm$. The result illustrates

the ability of the methodology to detect damage that is located close to one of the transducers of the network and is able to resolve the complex scatter signals which includes interference of scatter wave components from the transducer and the damage.

Case E4 considers the bonded mass located slightly outside the transducer network area. Figures 17a and b show the reconstructed damage localization image and corresponding binary image, respectively. The damage is detected and accurately located with a locating error smaller than $3\,mm$ which further proofs the robustness of the proposed Lamb wave based damage detection methodology for composite laminates.

4.2. Sensitivity study of group velocity error on the damage locating performance

This sub-section aims on studying the sensitivity of a potential group velocity error on the performance of the proposed damage detection methodology. The angular dependence group velocity can be obtained by using theoretically predicted or experimentally measured values. Both approaches may exhibit some error due to uncertain material parameters in the modeling for the theoretical prediction or measurement error in the experiment. Figure 18 shows the relation between the percentage error in the group velocity estimation and the damage locating error using the proposed methodology. The error of angular dependence group velocity is introduced by factorizing $\pm 10\%$ of the experimental measured group velocity for all directions. The figure shows that the proposed methodology is still able to predict the damage location within $5\,mm$ locating error for the group velocity error below $\pm 10\%$. This further highlights the robustness of the proposed damage detection methodology.

5. Conclusions

This paper presents an in-situ damage detection methodology for fiber-reinforced composite laminates utilizing Lamb waves. The proposed methodology has been verified in numerical and experimental case studies investigating the ability of the method to detect and locate

damage of different sizes and at different locations within the sensor network area.

The results show that the reconstructed binary damage image is able to accurately predict damage location and provides an estimation of the possible damage area even for relatively small damage and damage close to one of the network transducers or even slightly outside the transducer network. A major advantage of the proposed methodology is its robustness and efficiency considering that it requires only a few transducers to locate damage within and outside a 100 x 100 mm^2 sensor network area with locating errors of only a few millimeters, and the localization errors remain below 5 mm when uncertainties in the group velocity distribution of $\pm 10\%$ are assumed. As the proposed methodology only involves simple, numerically efficient cross-correlation analysis, it has the potential to enable real time, in-situ damage localization if it is used together with a multiplexed data acquisition system that allows the simultaneous collection of the response signals from different transducers and the sequential excitation of the transducers as transmitter elements. In summary, the study shows the potential of applying the proposed Lamb wave based damage detection methodology for in-situ structural health monitoring.

Current investigations are focusing on experimental studies to determine the reconstruction error for different types of damage, in particular delaminations and numerical and experimental studies to apply the method to complex composite structures, in particular laminates with stiffeners.

Acknowledgements

C.T. Ng would like to acknowledge the financial support from the University of Queensland Research Scholarship (UQRS), University of Queensland International Research Award (UQIRA) and Cooperative Research Centre for Advanced Composite Structures (CRC-ACS) Limited.

References

ABAQUS Theory Manual Version 6.7 2007 (ABAQUS, Inc.)

Alleyne D, and Cawley P 1991 A two-dimensional Fourier transform method for the measurement of propagating multimode signals *J. Acoust. Soc. Am.* **89** 1159-68

Boller C 2000 Next generation structural health monitoring and its integration into aircraft design *Int. J. Syst. Sci.* **31** 1333-49

Cawley P and Adams R D 1979 The location of defects in structures from measurements of natural frequencies *J. Strain Analysis for Engineering Design* **14** 49-57

Cegla F B, Rohde A and Veidt M 2008 Analytical prediction and experimental measurement for mode conversion and scattering of plate waves at non-symmetric circular blind holes in isotropic plates *Wave Motion* **45** 162-177.

Curtis T E and Ward R J 1980 Digital beamforming for sonar system *IEE Proc.* **127** 257-65

Diamanti K, Hodgkinson J M and Soutis C 2004 Detection of low-velocity impact damage in composite plates using Lamb waves *Structural Health Monitoring an Int. J.* **3** 33-41

Diamanti, K, Soutis C and Hodgkinson, J M 2007 Piezoelectric transducer arrangement for the inspection of large composite structures *Composites A* **38** 1121-30

Ghorayeb S R, Lord W and Udpa S S 1994 Application of a beamforming technique to ultrasound imaging in non-destructive testing *IEEE Trans.Ultrason., Ferroelectr. Freq. Control* **41** 199-208.

Giurgiutiu V and Bao J J 2004 Embedded-ultrasonics structural radar for in situ structural health monitoring of thin-wall structures *Structural Health Monitoring an Int. J.* **3** 121-40.

Ihn J B and Chang F K 2008 Pitch-catch active sensing methods in structural health monitoring for aircraft structures *Structural Health Monitoring an Int. J.* **7** 5-15

Lam H F and Ng C T 2008 A probabilistic method for the detection of obstructed cracks of

beam-type structures using spatial wavelet transform *Probabilistic Engineering Mechanics* **23** 237-245

Lam H F, Ng C T and Veidt M 2007 Experimental characterization of multiple cracks in a cantilever beam utilizing transient vibration data following a probabilistic approach *J. Sound Vib.* **305** 34-49

Lin X and Yuan F G 2001 Damage detection of a plate using migration technique *J. Intell Mater. Syst. Struct.* **12** 469-82

Litva J and Lo T K Y 1996 *Digital beamforming in wireless communications* (Artech House, Norwood, MA)

Mallet L, Lee B C, Staszewski W J and Scarpa F 2004 Structural health monitoring using scanning laser vibrometry: II. Lamb waves for damage detection *Smart Mater. Struct.* **13** 261-269.

Michaels J E and Michaels T E 2007 Guided wave signal processing and image fusion for in situ damage localization in plates *Wave Motion* **44** 482-92

Olson S E, DeSimio M P and Derriso M M 2007 Beamforming of Lamb waves for structural health monitoring *Trans. ASME* **129** 730-38

Pavlakovic B and Lowe M 2003 DISPERSE User's Manual Version 2.0.16B *Imperial College, University of London, Non-Destructive Testing Laboratory*.

Pratt W K 1991 *Digital image processing* (John Wiley & Sons, Inc. New York)

Raghavan A and Cesnik C E S 2007 Review of guided-wave structural health monitoring *The Shock and Vibration Digest* **39** 91-114

Rohde A, Veidt M, Rose L R F and Homer J 2007 Imaging flexural inhomogeneities using plate-wave diffraction tomography *The 33rd Annual Review of Progress in Quantitative Nondestructive Evaluation*, vol. 894 (Portland American Institute of Physics) p 673.

Santoni G B, Yu L, Xu B and Giurgiutiu V 2007 Lamb wave-mode tuning of piezoelectric wafer active sensors for structural health monitoring *Trans. ASME*, **129** 752-762

Staszewski W J, Boller C and Tomlinson G 2004 *Health monitoring of aerospace structures: smart sensor technologies and signal processing* (John Wiley & Sons Ltd, West Sussex)

Su Z, Cheng L, Wang X and Yu L 2008 Diagnostic imaging for structural damage *Adv. Mater. Res.***47-50** 157-60

Su Z, Ye L and Lu Y 2006 Guided Lamb waves for identification of damage in composite structures: A review *J. Sound Vib.* **295** 753-80

Sundararaman S, Adams D E and Rigas E J 2005 Structural damage identification in homogeneous and heterogeneous structures using beamforming *Structural Health Monitoring an Int. J.* **4** 171-90

Veidt M, Ng C T, Hames S and Wattinger T 2008 Imaging laminar damage in plates using Lamb wave beamforming *Adv. Mater. Res.* **47-50** 666-69

Veidt, M, Liu, T and Kitipornchai S 2001 Flexural waves transmitted by rectangular piezoceramic tranducers *Smart Mater. Struct*, **10** 681-688

Wang C H and Chang F K 2005 Scattering of plate waves by a cylindrical inhomogeneity *J. Sound Vib.* **282** 429-51

Wang C H, Rose J T and Chang F K 2004 A synthetic time-reversal imaging method for structural health monitoring *Smart Mater. Struct.* **13** 415-23

Worden K, Farrar C R, Manson G and Park G 2007 The fundamental axioms of structural health monitoring *Proc.Roy. Soc. A* **463** 1639-64

Zhao X, Gao H, Zhang G, Ayhan B, Yan F, Kwan C and Rose J L 2007 Active health monitoring of an aircraft wing with embedded piezoelectric sensor/actuator network: I. Defect detection, localization and growth monitoring *Smart Mater. Struct.* **16** 1208-17

Tables

Table 1. Elastic properties of lamina in the numerical case studies.

Properties	Value
E_{11}	152 GPa
E_{22}	9.5 GPa
E_{33}	9.5 GPa
G_{12}	4.2 GPa
G_{13}	4.2 GPa
G_{23}	3.4 GPa
ν_{12}	0.3
ν_{13}	0.3
ν_{23}	0.38
Density	1540 kg/m^3

Table 2. Geometric and material properties of piezoelectric transducer in the numerical case studies.

Properties	Value
Diameter	5 mm
Thickness	2 mm
Young's modulus	75 GPa
Density	7.7 g/cm^3
Poisson's ratio	0.3

Table 3. Summary of all cases and damage detection results in numerical case studies.

Case	True damage location $(x_d,\ y_d)\,mm$	True damage diameter (mm)	Predicted damage location $(x_c,\ y_c)\,mm$	Damage locating error E (mm)
N1	(135.00, 135.00)	2.00	(135.32, 135.95)	1.00
N2	(135.00, 135.00)	1.00	(135.46, 135.99)	1.09
N3	(135.00, 135.00)	0.50	(134.69, 136.42)	1.45
N4	(155.00, 145.00)	1.00	(153.60, 149.65)	4.85
N5	(175.00, 130.00)	1.00	(175.09, 127.66)	2.34

Table 4. Summary of all cases and damage detection results in experimental case studies.

Case	True bonded mass location (x_d , y_d) mm	True bonded mass diameter (mm)	Predicted bonded mass location (x_c , y_c) mm	Damage locating error E (mm)
E1	(55.00, 60.00)	10.00	(55.01, 60.17)	0.17
E2	(55.00, 60.00)	5.00	(57.97, 56.69)	4.44
E3	(10.00, 80.00)	5.00	(7.92, 79.73)	2.09
E4	(55.00, 90.00)	5.00	(55.86, 92.86)	2.98

Figures

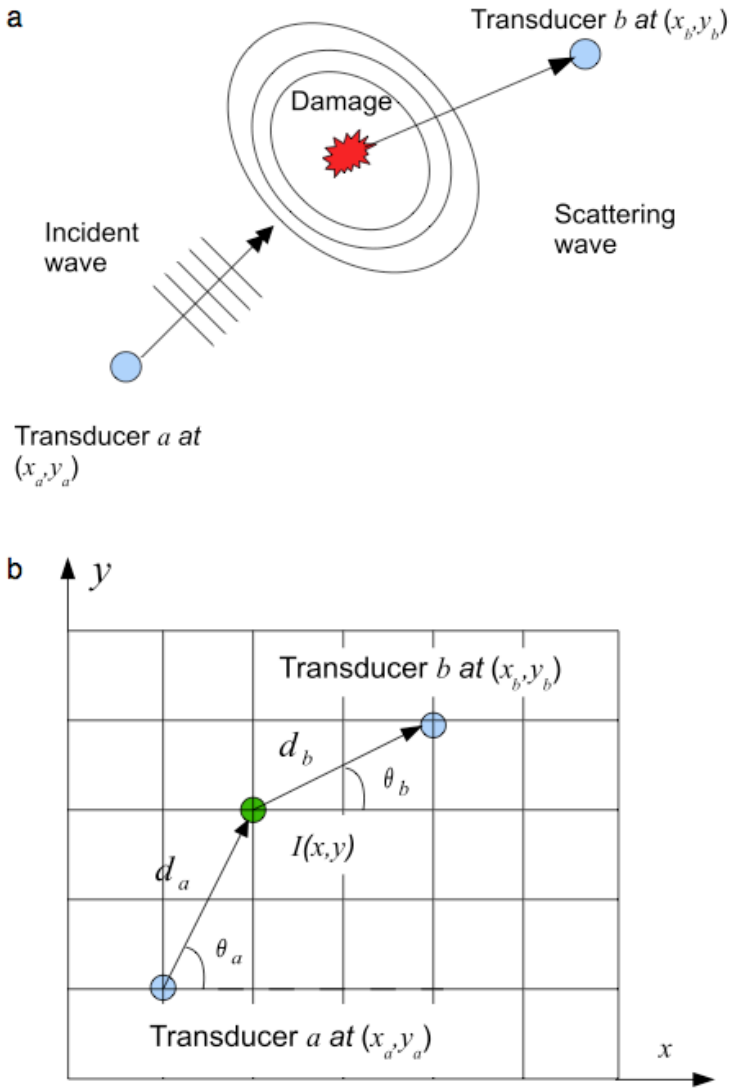

Figure 1. Lamb wave based damage detection methodology (a) wave scattering at damage, (b) characteristic parameters of the proposed image reconstruction algorithm for anisotropic material.

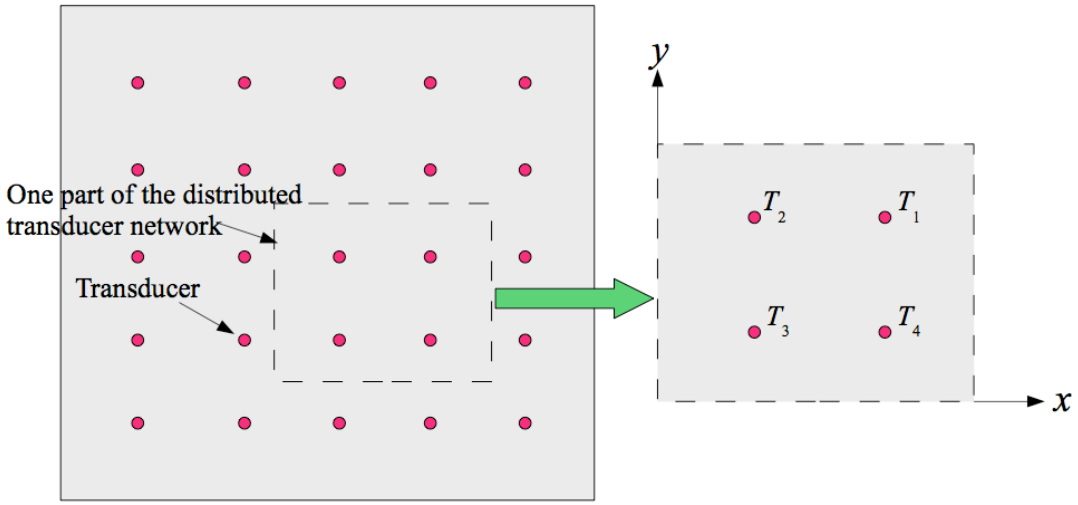

Figure 2. Possible distributed transducer network on a composite panel and representative part of the network used in current study.

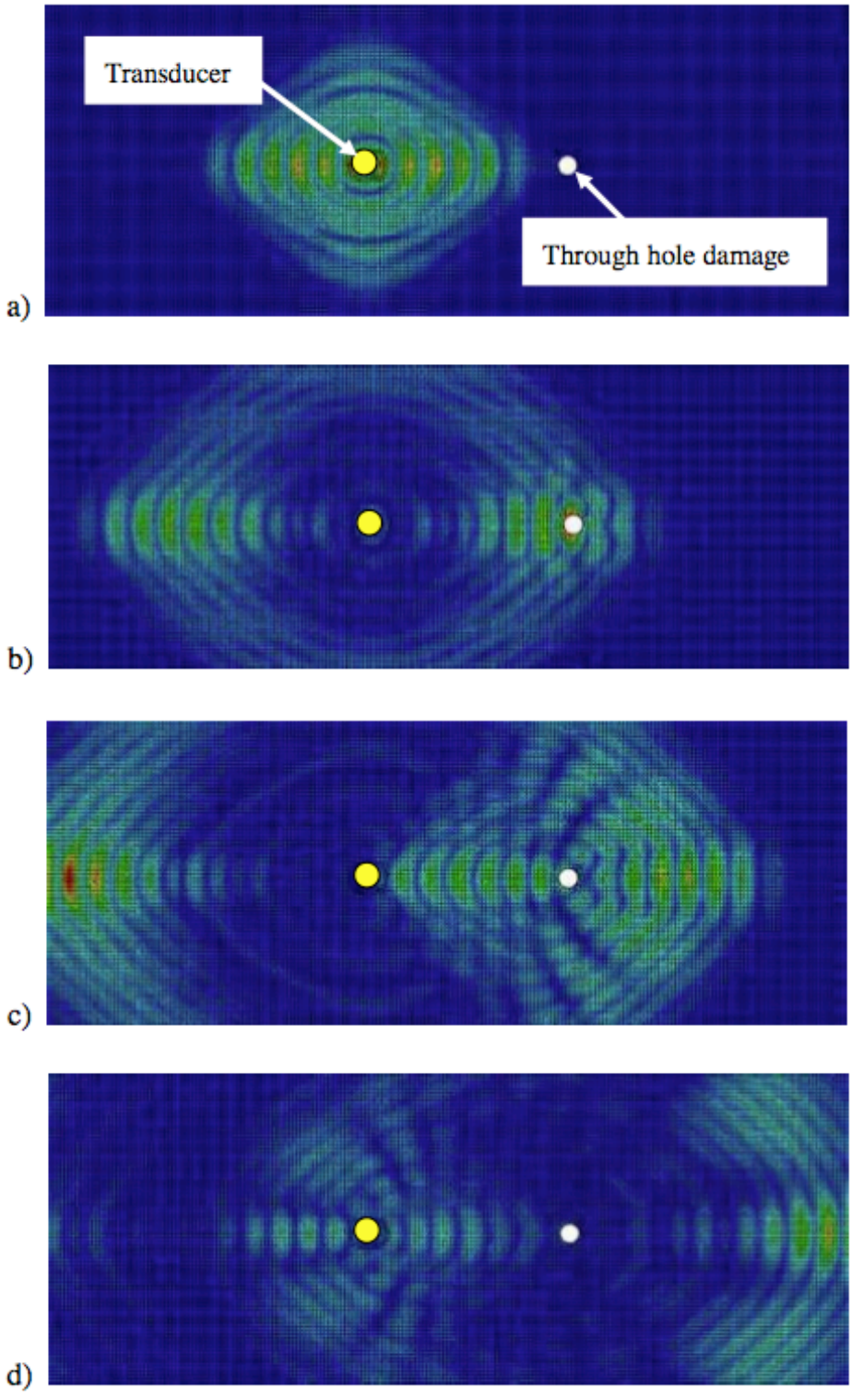

Figure 3. Snapshots of the out-of-plane displacement of propagating and scattered Lamb waves at (a) 15.8 μs , (b) 26.8 μs , (c) 36.8 μs and (d) 51.1 μs .

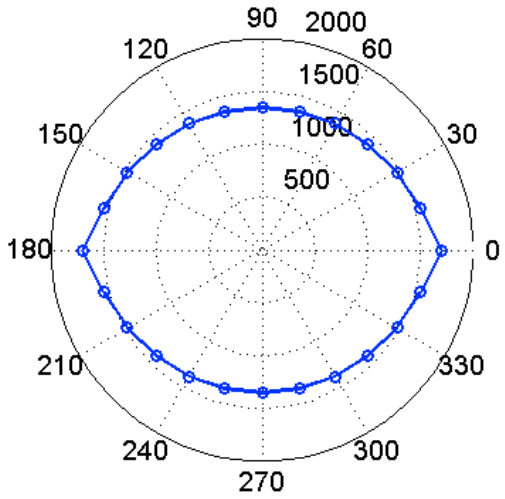

Figure 4. Angular dependence of group velocity in m/s for the 8-ply $[0_8]$ carbon fiber-reinforced laminate.

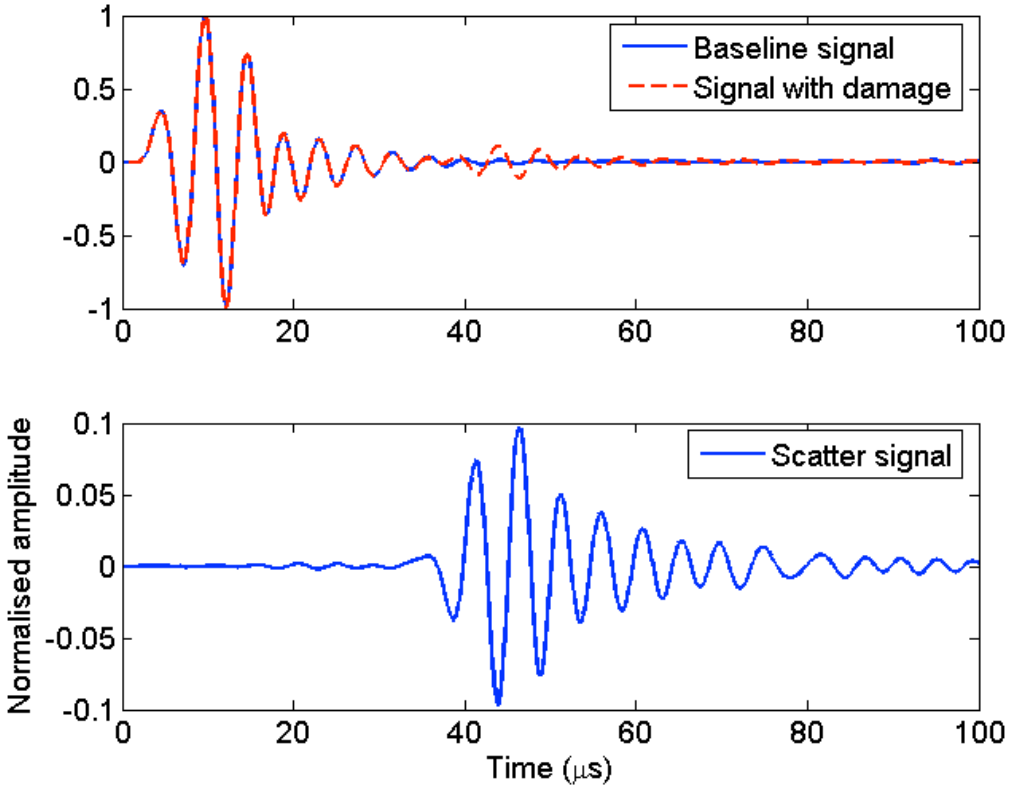

Figure 5. Typical baseline signal, signal with damage and calculated scatter signal from the finite element simulation.

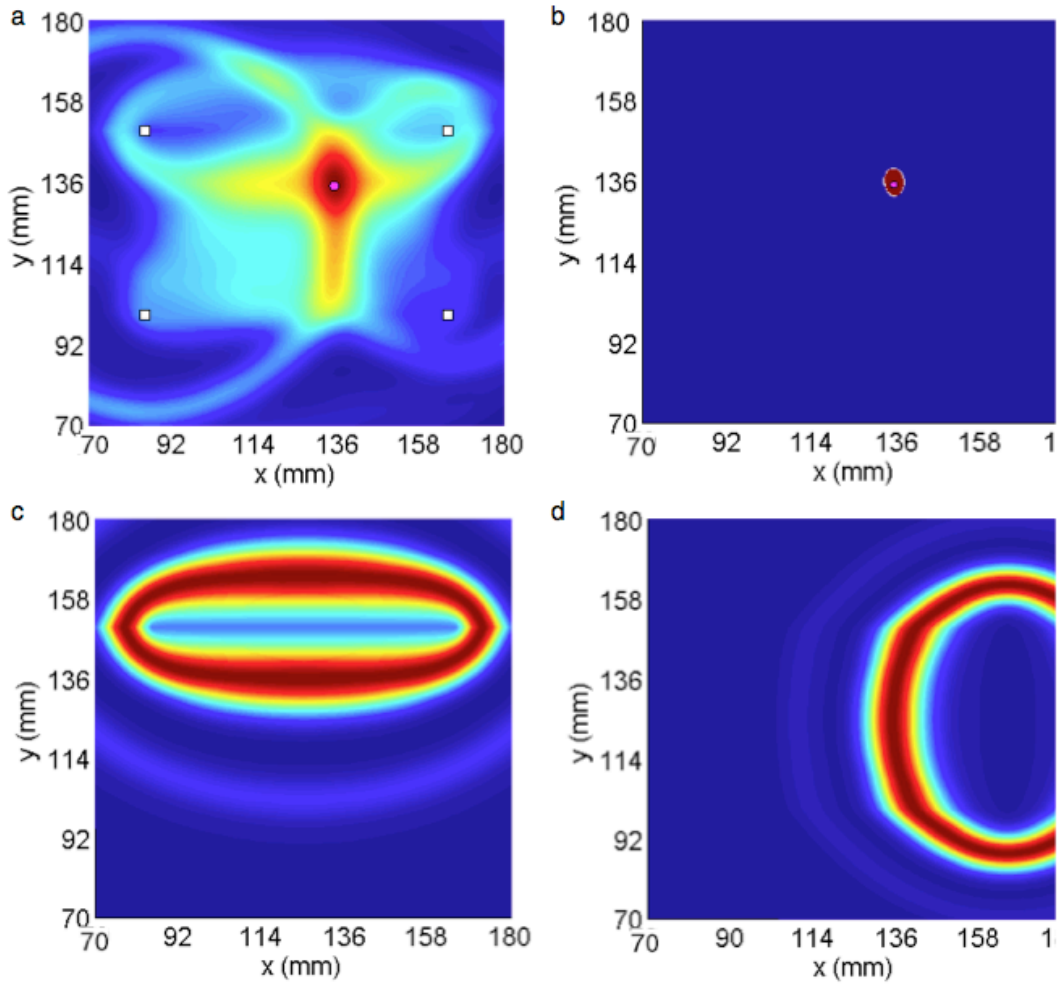

Figure 6. (a) Reconstructed damage localization image of case N1, (b) corresponding binary image, typical image of actuator/sensor signal paths (c) T1–T2 and (d) T1–T4.

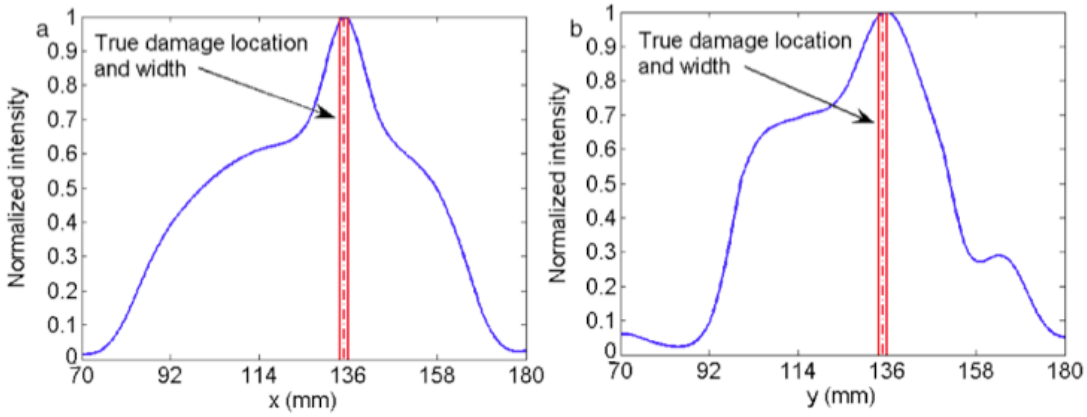

Figure 7. Sectional view of the reconstructed damage localization image along (a) x and (b) y axis through the actual damage position for case N1.

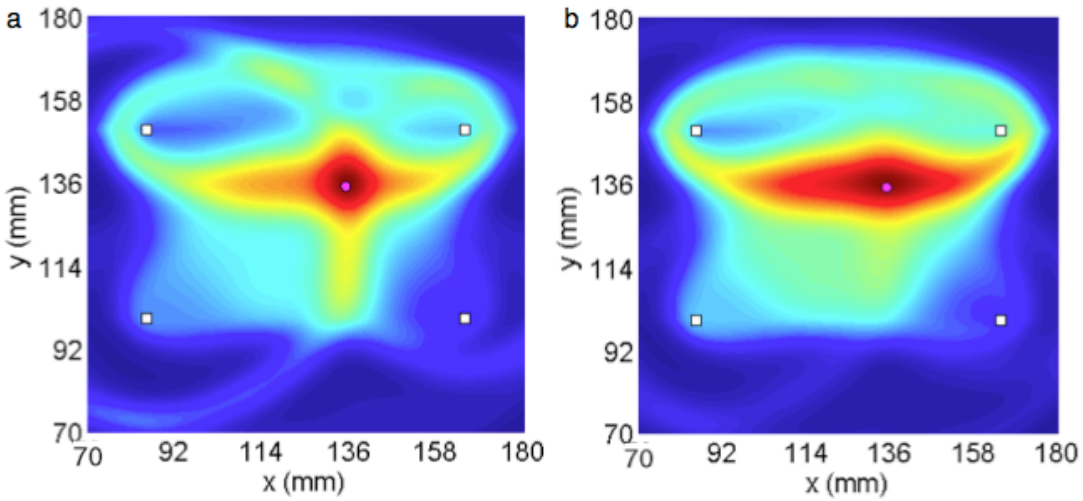

Figure 8. Reconstructed damage localization image of (a) case N2 and (b) case N3.

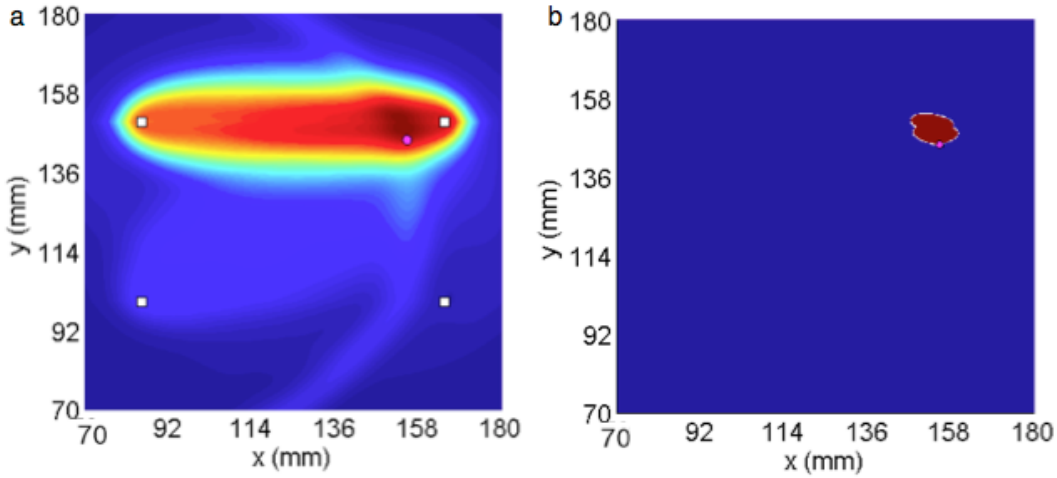

Figure 9. (a) Reconstructed damage localization image of case N4, (b) corresponding binary image.

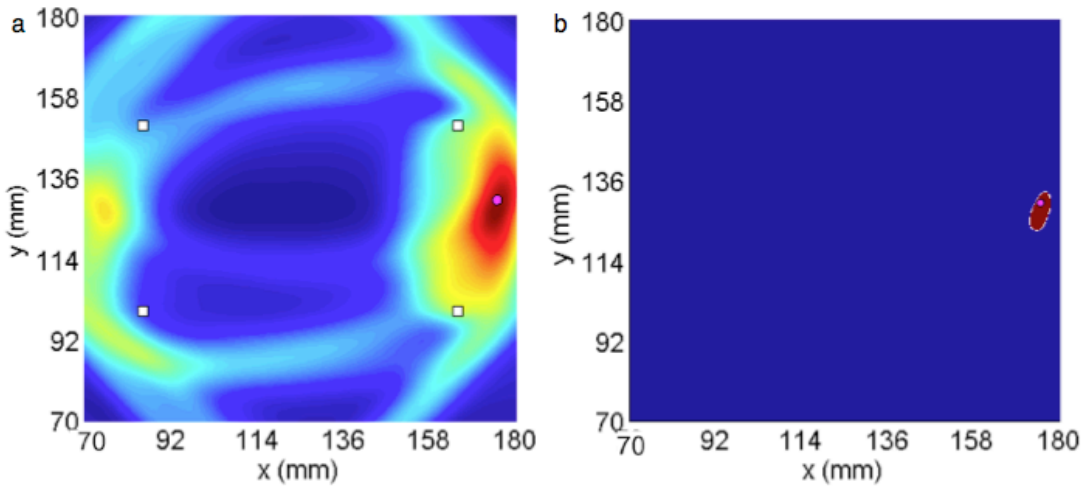

Figure 10. (a) Reconstructed damage localization image of case N5, (b) corresponding binary image.

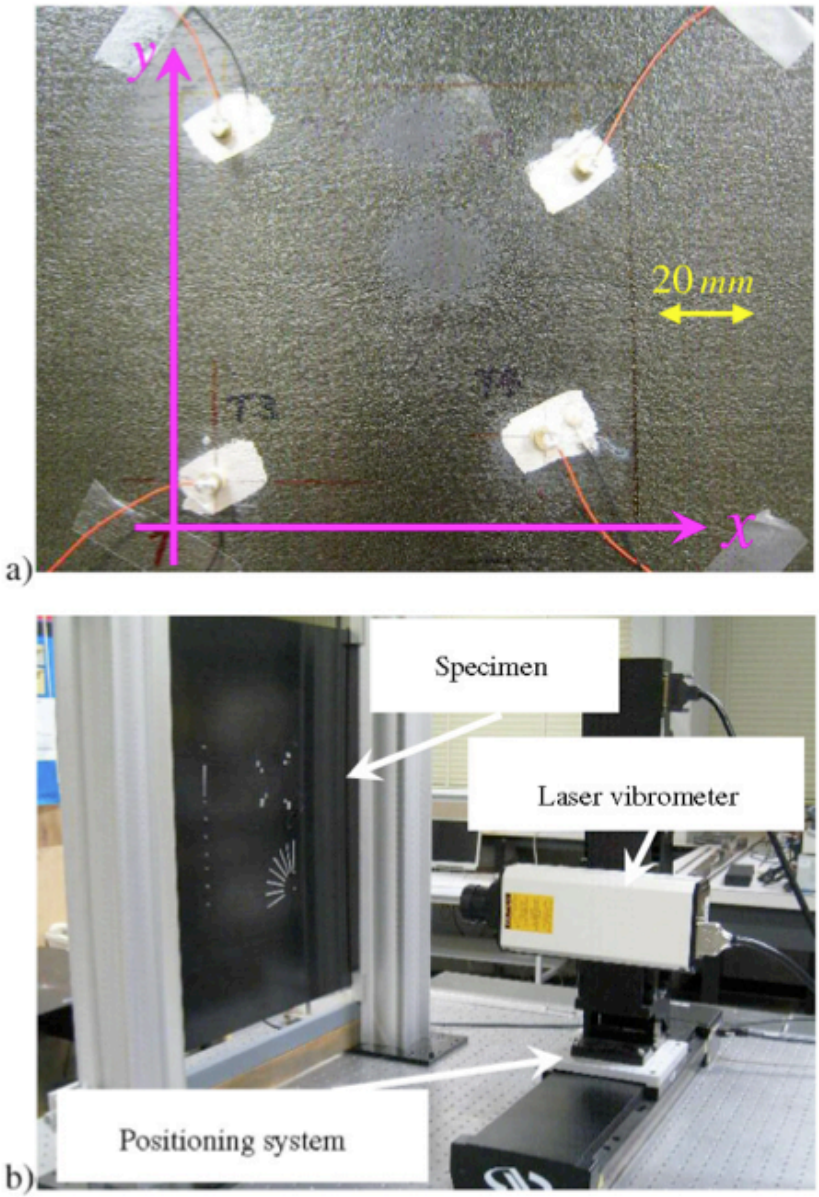

Figure 11. (a) Piezoceramic disk actuator installed on the composite laminate and (b) experimental set-up.

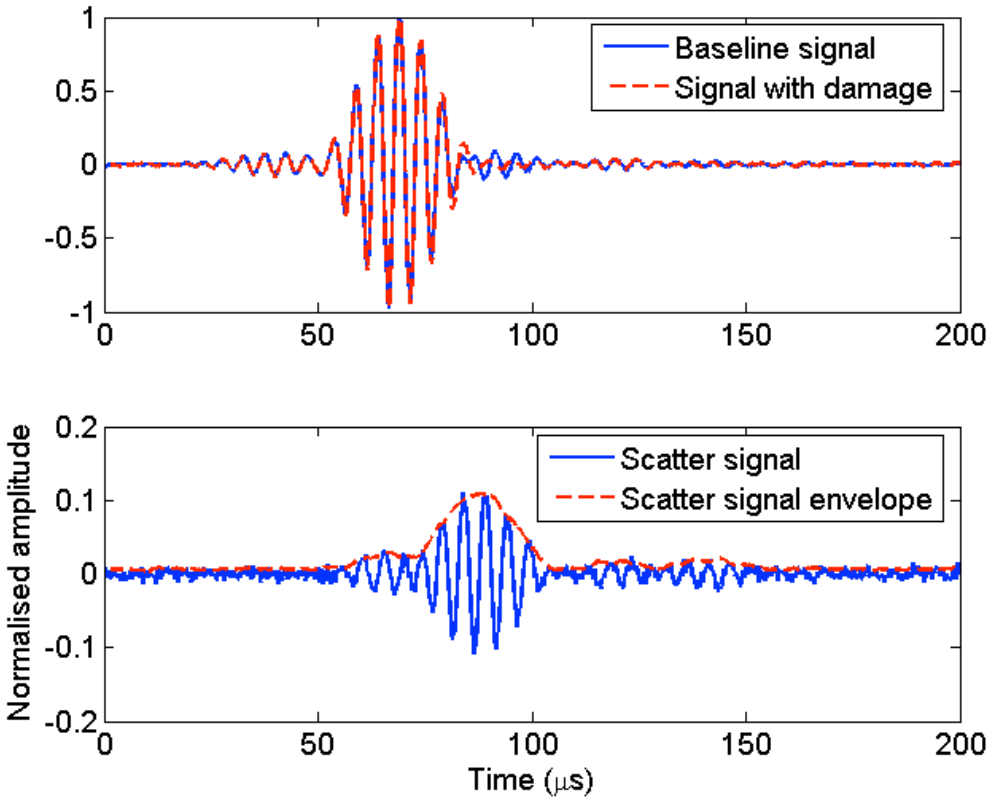

Figure 12. Baseline signal, signal with damage, scatter signal and corresponding envelope of signal path T3 – M2 of composite laminate with a 10 mm diameter bonded mass.

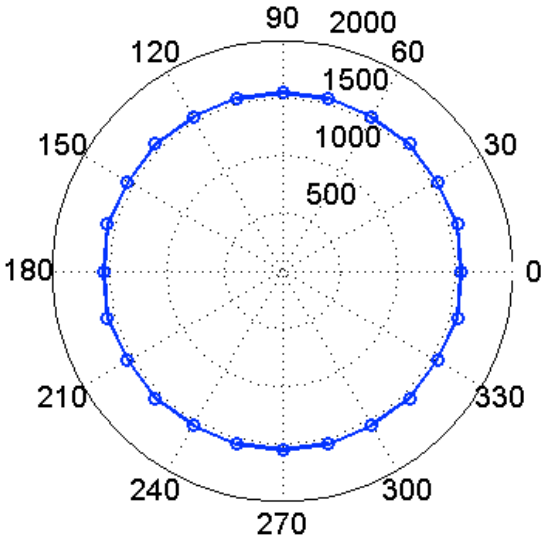

Figure 13. Angular dependence of group velocity in m/s for the 16-ply $[(0/90)_4]_s$ carbon fiber-reinforced laminate.

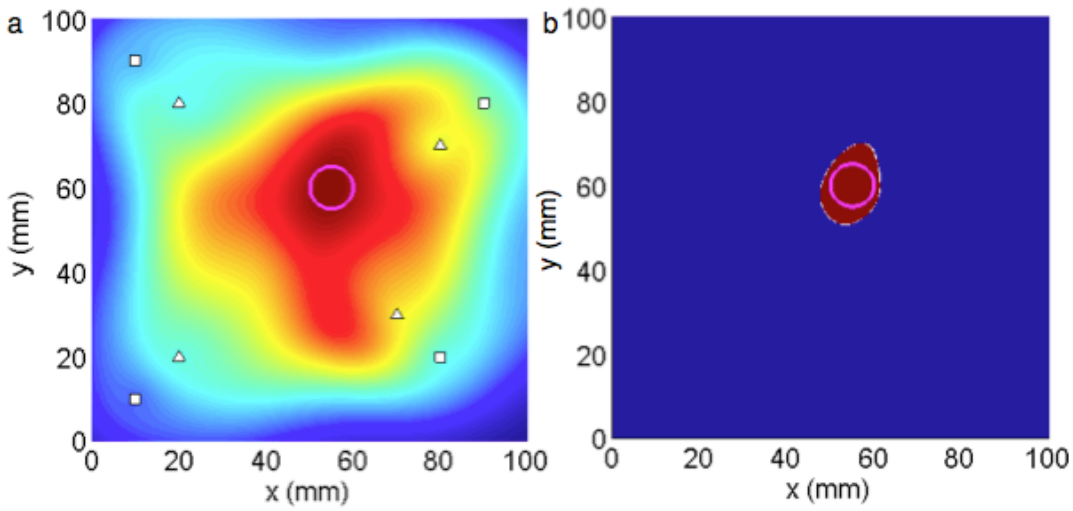

Figure 14. (a) Reconstructed damage localization image of case E1, (b) corresponding binary image.

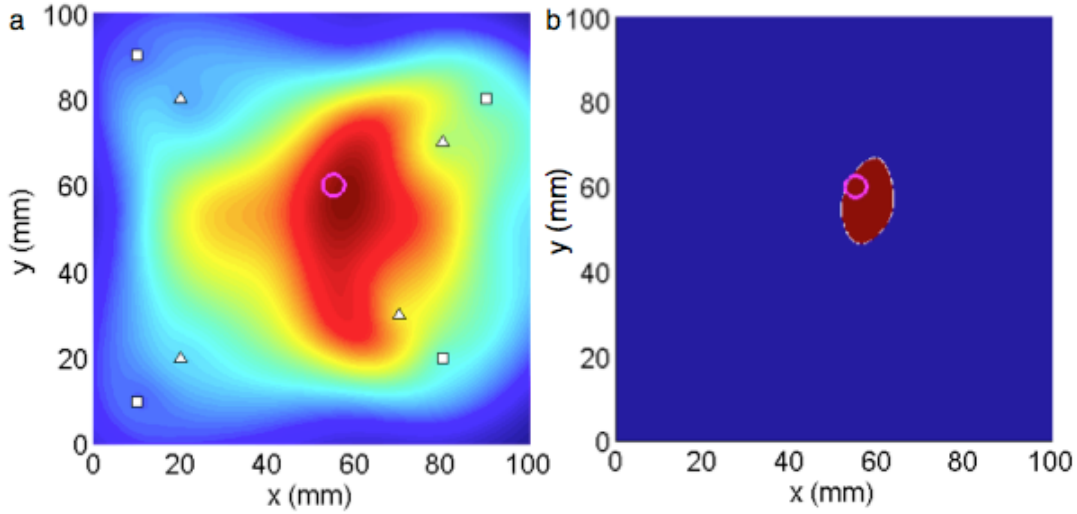

Figure 15. (a) Reconstructed damage localization image of case E2, (b) corresponding binary image.

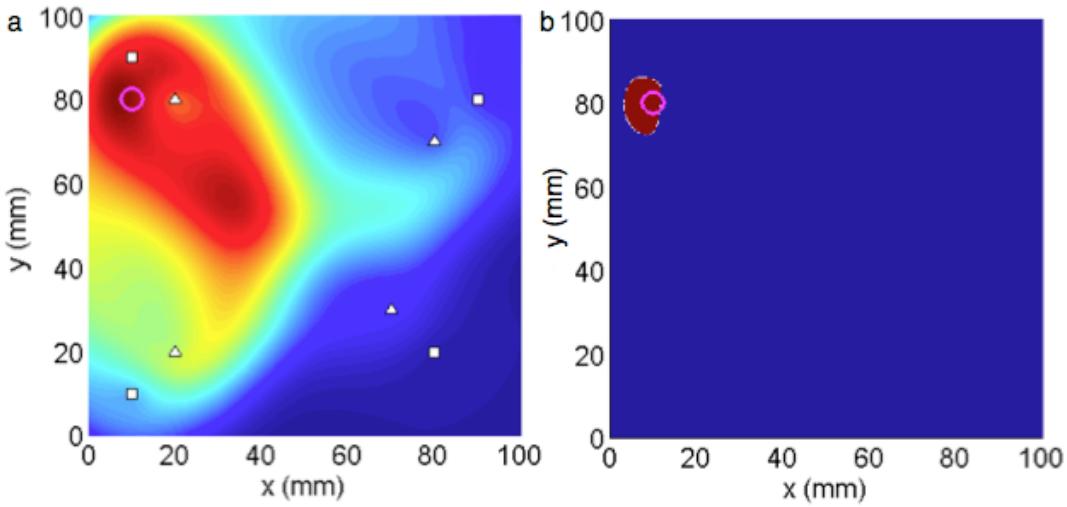

Figure 16. (a) Reconstructed damage localization image of case E3, (b) corresponding binary image.

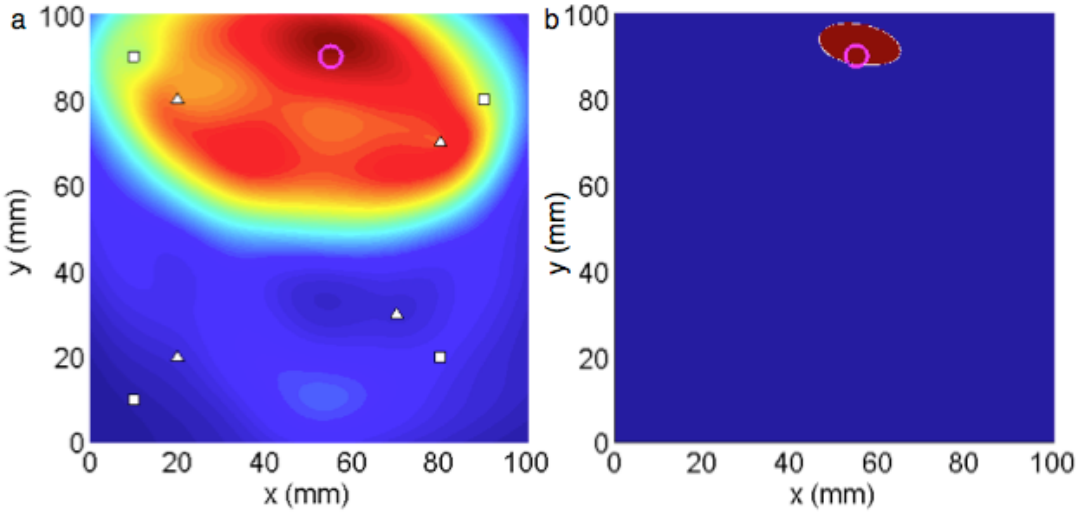

Figure 17. (a) Reconstructed damage localization image of case E4, (b) corresponding binary image.

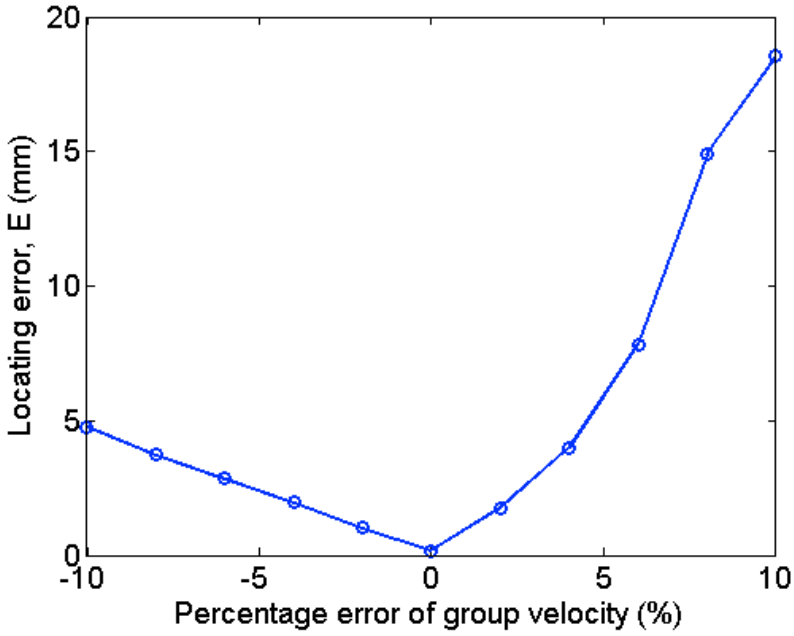

Figure 18. Relation between percentage error in group velocity estimation and locating error.